

#### **RESEARCH ARTICLE**

# The cellular function of ROP GTPase prenylation is important for multicellularity in the moss *Physcomitrium patens*

Liang Bao\*,1,‡, Junling Ren\*,1, Mary Nguyen¹, Arkadiusz Slawomir Slusarczyk², Julie M. Thole³, Susana Perez Martinez¹, Jinling Huang⁴, Tomomichi Fujita⁵ and Mark P. Running¹,‡

#### **ABSTRACT**

A complete picture of how signaling pathways lead to multicellularity is largely unknown. Previously, we generated mutations in a protein prenylation enzyme, GGB, and showed that it is essential for maintaining multicellularity in the moss Physcomitrium patens. Here, we show that ROP GTPases act as downstream factors that are prenylated by GGB and themselves play an important role in the multicellularity of P. patens. We also show that the loss of multicellularity caused by the suppression of GGB or ROP GTPases is due to uncoordinated cell expansion, defects in cell wall integrity and the disturbance of the directional control of cell plate orientation. Expressing prenylatable ROP in the ggb mutant not only rescues multicellularity in protonemata but also results in development of gametophores. Although the prenylation of ROP is important for multicellularity, a higher threshold of active ROP is required for gametophore development. Thus, our results suggest that ROP activation via prenylation by GGB is a key process at both cell and tissue levels, facilitating the developmental transition from one dimension to two dimensions and to three dimensions in *P. patens*.

KEY WORDS: Protein prenylation, ROP GTPase, Evolution, Land plants, Unicellular, Multicellularity, Cell expansion, Cell wall integrity

#### INTRODUCTION

Multicellularity has arisen multiple times and has given rise to many significant life forms, including plants, animals and fungi (Knoll, 2011; Niklas, 2014). Considerable research has recently focused on the barriers and drivers of that transition (Brunet and King, 2017; Cavalier-Smith, 2017; Heaton et al., 2020; Holmes et al., 2013; Kawabe et al., 2019; Knoll, 2011; Niklas and Newman, 2020; Pentz et al., 2020; Ratcliff et al., 2013; Rokas, 2008). Several requirements for the evolution of multicellularity have been proposed, most prominently including cell-cell adhesion and cell-cell communication (Kawabe et al., 2019; Rokas, 2008; Seymour et al., 2004). All eukaryotic cells can secrete polysaccharides and structural glycoproteins that self-assemble to form extracellular

<sup>1</sup>Department of Biology, University of Louisville, Louisville, KY 40208, USA.
<sup>2</sup>Department of Anatomical Sciences & Neurobiology, University of Louisville, Louisville, KY 40202, USA. <sup>3</sup>Department of Biology, Saint Louis University, St Louis, MO 63103, USA. <sup>4</sup>Department of Biology, East Carolina University, Greenville, NC 27858. <sup>5</sup>Faculty of Science, Hokkaido University, Sapporo 060-0810, Japan. <sup>\*</sup>Present address: Philips Institute for Oral Health Research, Virginia Commonwealth University, Richmond, VA 23298-0566, USA.

<sup>‡</sup>Authors for correspondence (mark.running@louisville.edu; liang.bao2005@gmail.com)

**L.B.**, 0000-0002-0228-6124; J.R., 0000-0002-8124-102X; M.N., 0000-0002-2188-3338; J.H., 0000-0003-4893-4171

Handling Editor: Ykä Helariutta

Received 2 November 2021; Accepted 24 May 2022

matrices (ECM), although the compositions of the ECM varies among lineages (Niklas and Newman, 2020). The establishment and maintenance of the stable cellular connections between and around neighboring cells that are necessary for the structural integrity of the ECM are key areas of research for all multicellular organisms (Abedin and King, 2010; Niklas and Newman, 2020). In animals, there are essentially four types of intercellular junctions in epithelial cells: adherens junctions, tight junctions, gap junctions and desmosomes (Seymour et al., 2004). The animal Rho family GTPases, including RohA, Rac1 and CDC42, are key regulators of cadherin-mediated adherens junctions (McCormack et al., 2013). In mesoderm tissue, glycoproteins, including collagen, proteoglycans, lamins and fibronectin, organize and arrange tissue structures (Rozario and DeSimone, 2010).

In land plants, the cell wall is the dominant intercellular structure and is chiefly composed of glycans. A dividing cell creates a new cell wall that joins the existing side walls, resulting in the adherence of the two daughter cells after cell division (Smith, 2001). Indeed, gene families encoding cell wall/cell adhesion are expanded in *Volvox*, a more recently emerged multicellular lineage, compared with *Chlamydomonas*, its unicellular relative (Prochnik et al., 2010). On the other hand, flowering plants have various mechanisms for inducing cell separation when environments are appropriate (Jarvis et al., 2003), indicating that cell adhesion is under regulatory control and is required for maintaining plant structural integrity.

The development of the moss *Physcomitrium patens* starts from a spore or a protoplast, which are single, rounded cells. During germination (spore) or regeneration (protoplast), the single cells elongate and divide to form chloronemata, which contain numerous chloroplasts and have transverse cross walls; they then form caulonemata, which contain fewer chloroplasts and have oblique cross walls (Cove et al., 2006); both are linear cells with branches. From the chloronemata or caulonemata, the gametophore will develop, consisting of stem and leaves (Moody, 2019; Tang et al., 2020; Whitewoods et al., 2018). The linear organization of protonemal cells without branches is one dimensional; the protonemal cells with branches are two dimensional; and the gametophores are three dimensional (Moody et al., 2021).

Protein prenylation, in which a prenyl lipid group is added to a target protein to facilitate protein plasma membrane localization and protein-protein interactions (Crowell and Huizinga, 2009; Running, 2014), is known to affect differentiation processes in *Arabidopsis* (Galichet and Gruissem, 2006; Running et al., 2004) and *P. patens* (Thole et al., 2014). There are two prenylation enzymes, farnesyltransferase (PFT) and geranylgeranyltransferase I (PGGT-I), that can recognize the C-terminal CaaX/CaaL four amino acid sequence [CaaX box; where 'C' is the prenylated cysteine, 'a' is usually an aliphatic amino acid, and 'X' is usually alanine, cysteine, glutamine, methionine or serine for PFT and almost always leucine (i.e. CaaL box) for PGGT-I] (Antimisiaris and Running, 2014).

Both PFT and PGGT-I consist of an  $\alpha$  subunit and  $\beta$  subunit, with a common  $\alpha$  subunit and distinct  $\beta$  subunits (Antimisiaris and Running, 2014). In contrast to the flowering plant Arabidopsis, in which ggb mutants (in which the PGGT-I  $\beta$  subunit is knocked out) have relatively mild phenotypes, resembling wild type under normal growth conditions (Johnson et al., 2005), ggb mutants in P. patens lose the processes of cell adhesion and cell differentiation, resembling unicellular algae (Thole et al., 2014). The downstream target(s) of GGB that are responsible for the cell-adhesion defects, and consequently for the multicellularity defects of ggb mutants in P. patens, are unknown.

#### **RESULTS**

## The cell wall of ggb mutants is disrupted due to uncoordinated cell expansion

Although we reported that multicellularity is lost in *ggb* mutants (Thole et al., 2014), we did not study how cell wall integrity might be affected during cell separation in this mutant. To achieve this, we used scanning electron microscopy (SEM) and transmission

electron microscopy (TEM) to visualize cell wall integrity. Rather than the smooth organization of the cell wall surface in wild type, the cell wall surface of ggb is disrupted, appearing to be torn apart (Fig. 1A,B). We could identify two distinct stages in ggb mutants: an early stage when the surface of cell wall attaches to more than 50% area of the cells; and a later stage when the surface of cell wall detaches from more than 50% of cells, as shown in live-imaging analysis (Fig. S1A,B). This indicates that the detachment of cells could be due to unregulated cell expansion. Wild-type protonema develop through tip growth, with the growing point localized to the tip region of the apical cells, as confirmed by microsphere experiments (Menand et al., 2007). Comparison of microsphere staining patterns between different time points allows us to detect the area of expansion on cell surfaces over time periods. No change in staining patterns on a cell surface area indicates no cell expansion is taking place, whereas a change in staining patterns indicates cell expansion. In contrast to wild type, in which expansion occurs only at the tip of apical cells or branching apical cells (n=7), the expansion of ggb is distributed over the entire cell, including

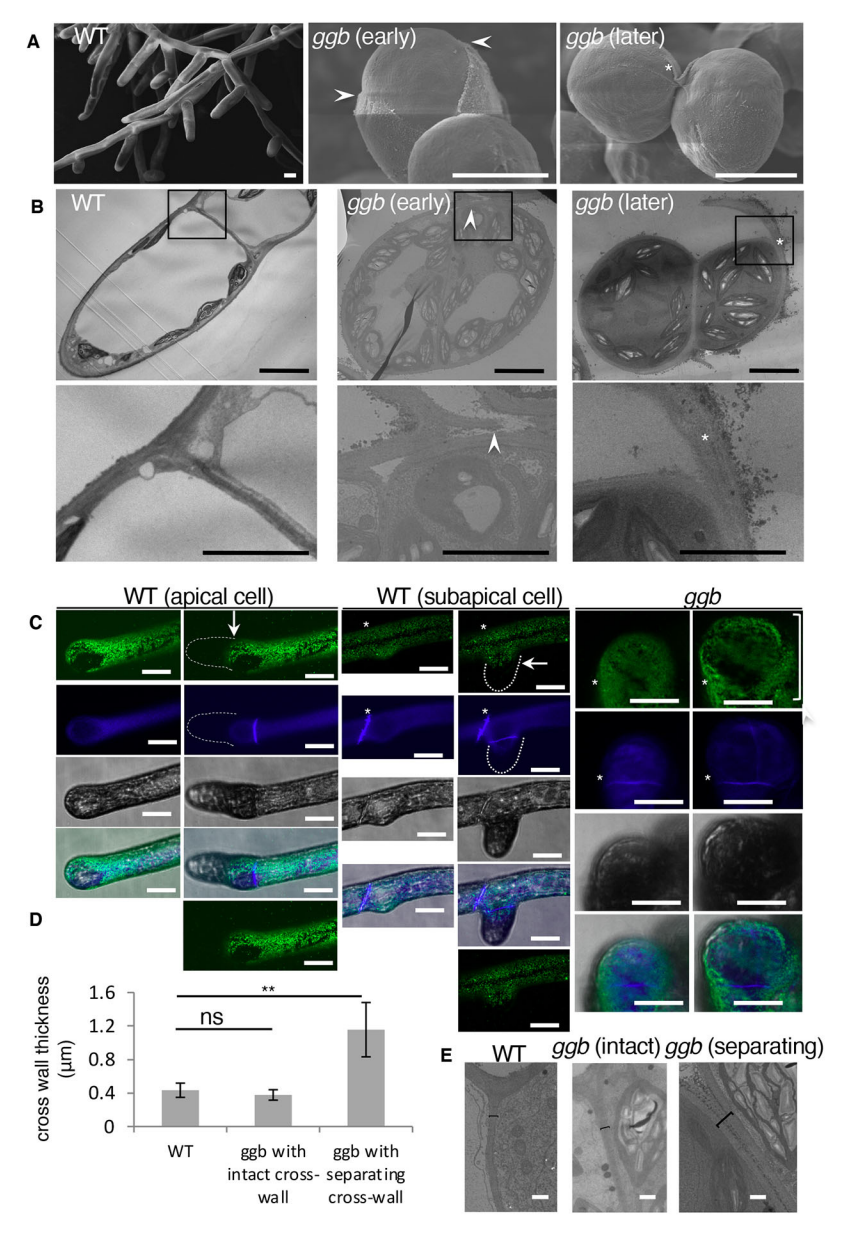


Fig. 1. ggb shows a unicellular-like lifestyle, due to uncontrolled cell expansion. (A,B) SEM (A) and TEM (B) of wild-type and ggb. For ggb, two images are shown for early and later development of cell separation. Scale bars: 20 µm (A), 10 μm (B, upper) and 5 μm (B, enlarged). Arrowheads indicate the broken surface cell walls in ggb mutants. Asterisks indicate the detaching cell wall surface in ggb mutants. (C) Dynamics of microspheres shown before (left) and after (right) a time interval (6 h for wild type and 24 h for ggb mutant). Four pictures are shown from top to bottom: microsphere (in green), calcofluor (in blue), brightfield (in gray) and overlay. Arrows indicate that the expansion occurred only at the tips of apical cells or the branching cell in wild type. Dashed lines indicate the edges of expanding tip in wild type and the same images of microsphere staining are provided at the bottom (the 5th row). Cell expansion (indicated by a bracket) was widespread across cells, including the cross walls, in qqb. Asterisks indicate the cross walls. Scale bars: 20 µm. (D) Comparing cross wall thicknesses of wild type, ggb mutant with intact cross walls and ggb mutant with separating cross walls. Data are mean±s.d. n=5 for wild type, n=7 for ggb with intact cross-wall and n=6 for ggb with separating cross walls. Differences were analyzed using Welch's t-test of mean. (E) Representative images of the cross walls of wild type, and of early and later stage gab mutants. Brackets indicate cross walls. Scale bars: 1 µm.

the peripheral regions and cross walls (n=4) (Fig. 1C). To further investigate the uncontrolled cell expansion in the cross wall region, we next checked the dynamics of cross walls during cell separation by comparing the thicknesses of the wild-type cross walls, the intact cross walls of gbb where neighboring cells tightly contact each other and the separating cross walls of gbb (Fig. 1D,E). We have measured the thickness of cross walls that are 2  $\mu$ m from the edge of side wall. Although cross wall thicknesses of wild type and tightly contacted cross walls of gbb were similar (P=0.2490), the thickness of the separating cross walls of gbb was almost three times greater than that of wild type (P=0.0021) (Fig. 1D). The above observations demonstrate that ggb mutants compensate for detached cross walls by increasing their thickness, as appropriate for the unicellular lifestyle of the mutant.

#### Uncontrolled cell expansion in ROP knockdown plants

We previously found that there are at least 61 proteins with a CaaL box in *P. patens*, of which 14 have no close homolog in *Arabidopsis* (Antimisiaris and Running, 2014). Among the 61 targets in *P. patens* are four ROPs (Rho of plant GTPases), all of which contain the CaaL box (Eklund et al., 2010). ROP protein knockdowns (Burkart et al., 2015; Yi and Goshima, 2020) and *rop*-null mutants (Cheng et al., 2020) of *P. patens* lose the processes of cell adhesion and cell differentiation, and thus ROPs would seem to be likely targets of protein prenylation (most likely geranylgeranylation) on the cysteine residue of the CaaL box by PGGT-I (Yalovsky, 2015).

Transgenic plants inducibly suppressing ROP expression by artificial microRNA (amiRNA) were generated using the XVE system (Kubo et al., 2013), introducing the PGX8-ROP-amiRNA into wild-type P. patens. Five ROP-amiRNA lines were obtained, each showing cell elongation defects upon induction by β-estradiol (Fig. S2A). Two of the five lines, numbers 15 and 26, showed the most severe phenotypes, including loss of cell adhesion (Fig. S2A). Therefore, ROP-amiRNA number 26 was used for further analysis in this study. RT-PCR showed all ROPs were downregulated in the ROP-amiRNA number 26 plants (Fig. S2B,C), and defects of cell elongation, cell division orientation and cell separation were observed after induction by  $\beta$ -estradiol (Fig. S3). Close examination of the surface by SEM showed that the cell wall of the ROP-amiRNA plants was also torn, similar to that of ggb mutants (Fig. 2A). The cell polarity marker YFP-AtRabA4d is specifically localized at the tip of the apical cell in protonemata, marking growth points of the apical cells in *P. patens* (Perroud and Quatrano, 2008). Compared with the tip localization of YFP-AtRabA4d protein in protonemata in wild type, YFP-AtRabA4d is uniformly present in cells of ggb mutants and ROP-amiRNA plants (Fig. 2B). Microtubule organization is dynamic, undergoing assembly and disassembly. During cell division, the overall organization of microtubules is similar among wild type, ggb mutants and ROPamiRNA plants in metaphase and cytokinesis (Fig. 2C), suggesting that cytokinesis is not affected, although the orientation of cell plate formation was defective in ggb mutants and in ROP-amiRNA plants (Fig. S3). Consistently, we found that, at interphase, whereas WT has a generally parallel orientation of microtubules, the ggb mutants and ROP-amiRNA plants have more randomized orientations of microtubules (Fig. S4).

## Prenylation of ROP GTPase is responsible for maintaining multicellularity

The similarities between *ROP-amiRNA* plants and *ggb* mutants (Fig. 2) prompted us to investigate further the relationships between GGB and ROPs; i.e. whether ROPs are genetically downstream of

GGB. Because, in *ggb* mutants, only PFT but not PGGT-I is active, we wanted to examine whether farnesylation of ROPs could compensate for the loss of PGGT-I.

To this end, we chose PpROP4 for this experiment, which is most highly expressed among all four ROPs in the wild-type P. patens (Fig. S2B). We have generated three YFP-tagged PpROP4 variants: YFP-PpROP4<sup>CVIM</sup>, with a consensus farnesyltransferase target motif; YFP-PpROP4CVIL, with a geranylgeranylation motif; and nonprenylatable YFP-PpROP4SVIL. We overexpressed them in the ggb mutant and in wild type. Eight to 12 lines of the three variants were obtained in wild-type and ggb mutant backgrounds, and lines with similar expression levels (determined using YFP florescent intensity as an indicator) for each variant were chosen for further analysis. As a control, the nonprenylatable YFP-PpROP4SVIL protein is not associated with the plasma membrane, and YFP-PpROP4<sup>SVIL</sup> overexpression does not affect cell morphology in wild type and ggb mutants (Fig. 3A,B, Fig. S5A,B). In contrast, YFP-PpROP4<sup>CVIM</sup> protein is mainly associated with the plasma membrane; YFP-PpROP4<sup>CVIM</sup> overexpression induces cell swelling in wild type and triggers tip growth and cell adhesion to form filamentous cells in ggb mutants (Fig. 3A,B, Fig. S5A,B). We also observed that YFP-PpROP4CVIL protein is mainly located in the plasma membrane in wild type, and in the plasma membrane, the cytosol and nucleus in ggb mutants, suggesting that YFP-PpROP4<sup>CVIL</sup> is partially farnesylated by PFT in ggb mutants. Similar to YFP-PpROP4CVIM but not YFP-PpROP4SVIL, YFP-PpROP4<sup>CVIL</sup> overexpression also causes cell swelling in wild type, consistent with the previous result for PpROP2 (Ito et al., 2014), and, interestingly, YFP-PpROP4CVIL overexpression also induced multicellularity with filamentous cells in ggb mutants (Fig. 3A,B, Fig. S5A,B). These results suggest that overexpressed PpROP4<sup>CVIM</sup> and PpROP4<sup>CVIL</sup> are farnesylated by PFT in ggb mutants (i.e. in the absence of PGGT-I) at sufficient levels to induce multicellularity.

Filamentous cells of moss show directional tip growth under polarized light (polarotropism) (Jenkins and Cove, 1983), and *ggb* mutants lack polarotropism (Thole et al., 2014). Prenylatable ROP overexpression in *ggb* produces filamentous cells that show polarized tip growth in response to polarized light (Fig. S6), indicating that ROP overexpression rescues *ggb* both morphologically and functionally. Therefore, our data suggest that ROPs work downstream of PFT and PGGT-I for establishment of multicellularity.

In ggb mutants (Thole et al., 2014) and rop-null mutants (Cheng et al., 2020), no gametophore forms. We asked whether activating ROPs could rescue the gametophore development defect of ggb mutants. We found that expressing YFP-PpROP4<sup>CVIM</sup> rescued the defects of both protonemal tip growth and gametophore development in ggb, although the rescued gametophores are substantially smaller than wild type at the mature stage (Fig. 3C). Although tip growth of ggb mutants is rescued when YFP-PpROP4<sup>CVIL</sup> is overexpressed, gametophores could not be generated in these plants (Fig. 3C). This is likely due to relatively higher activity of ROP<sup>CVIM</sup>, which is contains a more preferred PFT target sequence, compared with ROP<sup>CVIIL</sup>.

## Expressing prenylatable *Arabidopsis* AtROP1, but not human HsRAC1 and HsKRAS4b, rescues multicellular defects of *ggb* mutants

ROPs belong to the Ras superfamily of small GTPases that contains five major families: Ras, Rho, Arf/Sar, Ran and Rab, and plant ROPs are most closely homologous to RACs of the Rho family (Rojas et al., 2012), but ROPs form a single, distinct clade (Eklund et al., 2010).

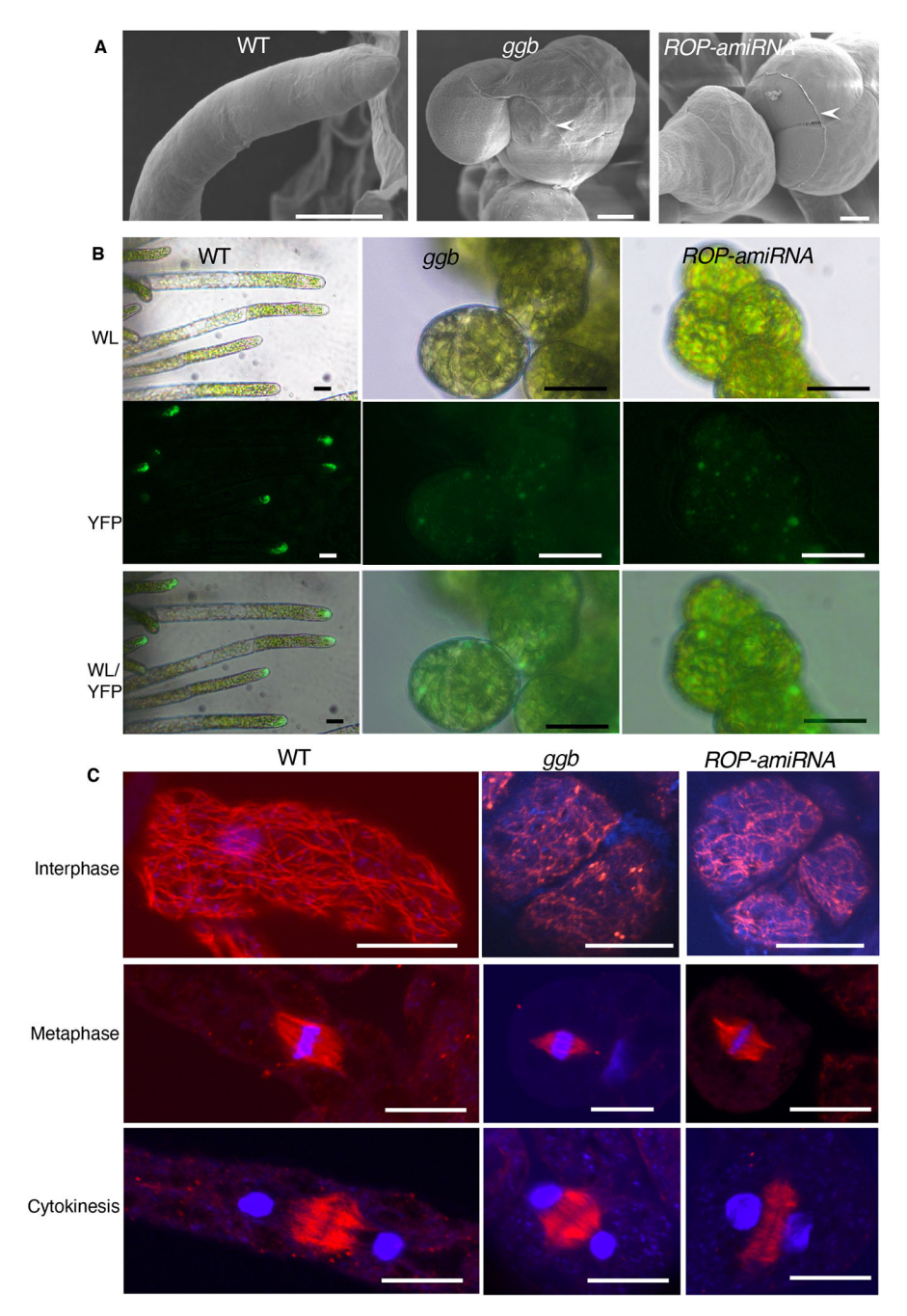


Fig. 2. Uncontrolled cell expansion in ROP knockdown plants compared with that in ggb mutants. (A) Representative SEM images of wildtype, ggb and ROP-amiRNA plants. ROPs-amiRNA plants form a single cell-like plant similar to the ggb mutant. Scale bars: 10 µm. Arrowheads indicate the broken surface cell walls in ggb mutants. (B) YFP-AtRabA4d expressed in wild-type, ggb and ROPamiRNA plants. YFP-AtRabA4d is present at the tip of an apical cell in wild type but is ubiquitously present in cells of gab and ROP-amiRNA plants. WL. white light: YFP, YFP-AtRabA4d; WL/YFP, overlay of WL and YFP. Scale bars: 20 µm. (C) Immunostaining of microtubules in wild-type, ggb and RO ROP-amiRNA plants at different stages of cell division. Red, microtubules; blue, DAPI. Scale bars: 20 µm.

Thus, we wanted to test whether the prenylation/ROP module function for multicellularity is conserved by expressing *Arabidopsis* AtROP1 and human HsRAC1 and HsKRAS4b in *ggb* mutants. AtROP1 and HsRAC1 belong to the Rho family and HsKRAS4b belongs to the RAS family (Rojas et al., 2012). All three proteins were YFP-tagged at the N-terminal and modified with CVIM at the C-terminal as a consensus farnesyltransferase target motif. Although all proteins are expressed at similar levels and associated with the plasma membrane, only YFP-AtROP1<sup>CVIM</sup> rescues tip growth and gametophore development defects in *ggb*; YFP-HsRAC1<sup>CVIM</sup> and YFP-HsKRAS4b<sup>CVIM</sup> do not (Fig. 4A,B).

#### DISCUSSION

In this study, we show that the breaking of cell walls in *ggb* mutants is due to uncontrolled cell expansion and/or defects in cell wall

integrity (Fig. 1 and Fig. S1). There are similarities between *ROP-amiRNA* plants and *ggb* mutants in terms of cell wall integrity (Fig. 2A), distribution of cell polarity marker (Fig. 2B), organization of overall microtubule orientation (Fig. 2C), cell division orientation (Fig. S3A,B) and directional tip growth to the external light signal (Fig. S6). Expressing prenylatable ROP in *ggb* mutants rescued its tip growth defect, resulting not only in multicellularity but also in the development of gametophores, which is not observed using nonprenylatable ROP (Fig. 3). Such genetic evidence prompts us to propose that the defects ROP activity are directly responsible for the unicellular phenotype observed in *ggb* mutants.

Interestingly, the *ggb* mutant phenotype shows some similarities to the *rop*-null mutant; however, unlike the very slow growth in *rop*-null mutants (Cheng et al., 2020), *ggb* mutants actively divide

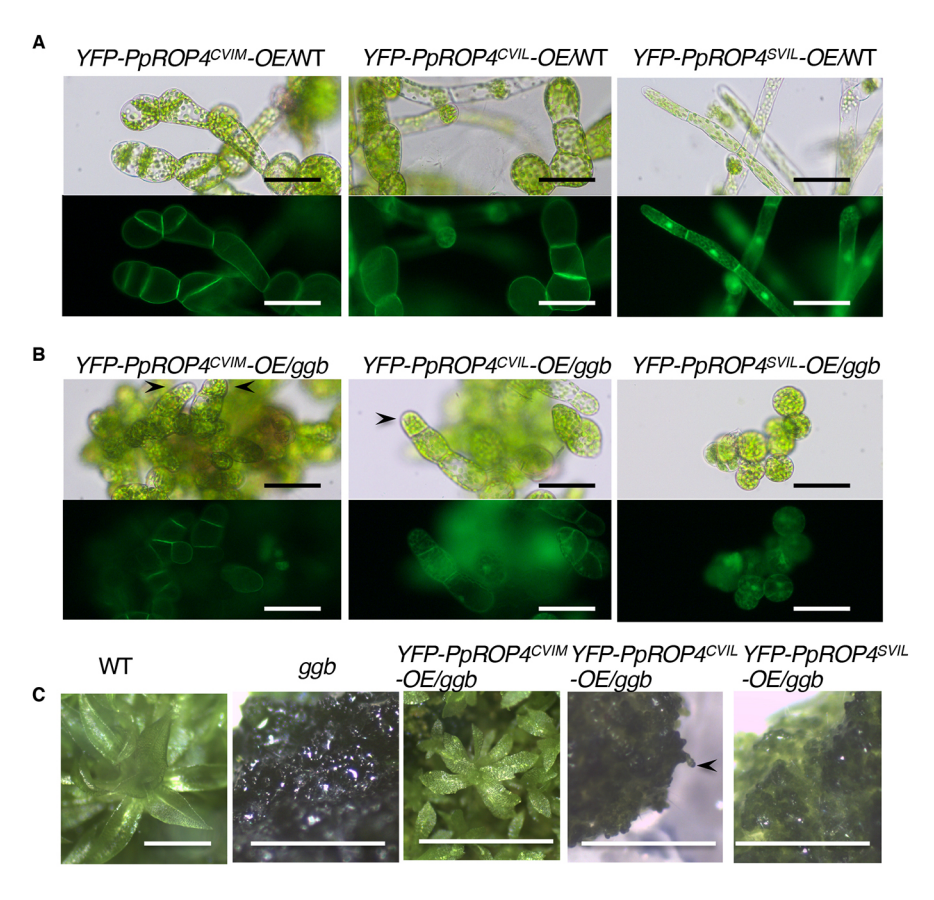


Fig. 3. Prenylation of ROP GTPase is responsible for maintaining multicellularity. (A,B) Representative images of transgenic plants overexpressing PpROP4CVIM, PpROP4CVIL and PpROP4<sup>SVIL</sup> in wild type (A) or in *ggb* mutants (B). The plants were grown in BCDAT with 1 μM β-estradiol for 7 days. Although overexpressing PpROP4CVIM or PpROP4<sup>CVIL</sup> resulted in swelling protonemal cells in wild type and rescued cell-adhesion defects in ggb mutants, overexpressing PpROP4<sup>SVIL</sup> did not. Arrowheads indicate rescue of tip growth defect of ggb. Scale bars: 100 μm. (C) The gametophore development defect of ggb was rescued by overexpressing PpROP4CVIM but not PpROP4CVIL or PpROP4<sup>SVIL</sup>. The plants were grown in BCDAT with 1 μM β-estradiol for 57 days. Scale bars: 1 mm. Arrowheads indicate the rescued tip growth.

(Thole et al., 2014). This difference might be due to the presence of farnesylation activity provided by PFT in the *ggb* mutant background, although the endogenous activation of ROPs by the PFT in the *ggb* mutant is not sufficient to establish normal morphogenesis of multicellularity (Fig. 5). In contrast, activating excessive ROPs in the *ggb* mutant initiated tip growth as well as gametophore development (Fig. 3). The data further suggest that, although low activity of ROP is sufficient for tip growth of filamentous protonema, higher activity of ROP is required for gametophore development (Fig. 5). Thus, our study suggests that

the prenylation/ROP module is pivotal for establishment of multicellularity through coordination of cell expansion, cell wall integrity and cell division orientation, and that prenylated ROP is important for controlling tissue complexity (Fig. 5).

By comparing the related Ras superfamily genes from other organisms, including humans, we show that, among those tested, only *Arabidopsis* AtROP1 rescues multicellular defects of *ggb* mutants (Fig. 4), suggesting the conserved molecular function of ROPs between *Arabidopsis* and *P. patens*, but not a general conservation among Rho GTPases or other GTPases of the RAS

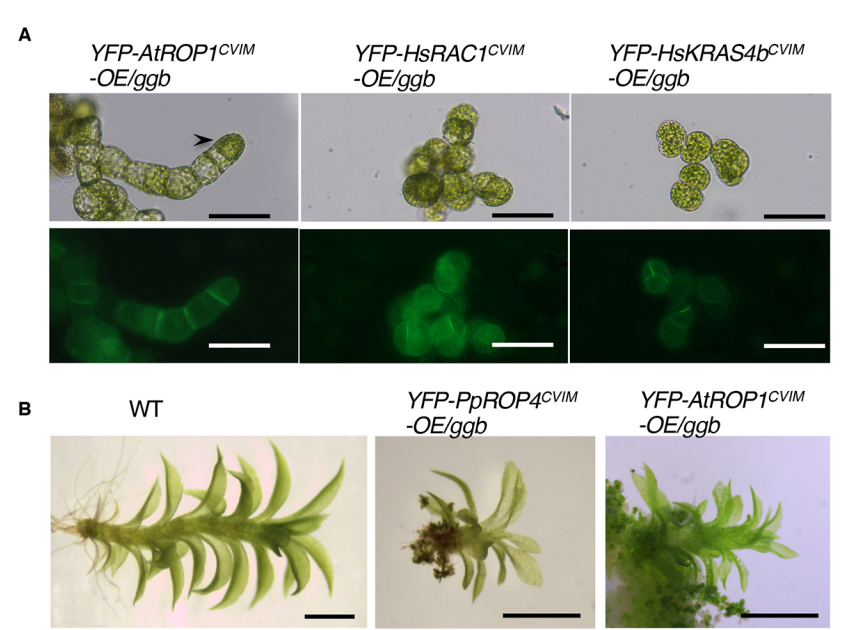


Fig. 4. Expressing prenylatable *Arabidopsis* AtROP1 rescues multicellular defects of *ggb* mutants. (A) The tip growth defects of *ggb* are rescued by the YFP-tagged *Arabidopsis* AtROP1<sup>CVIM</sup>, but not by human HsRAC1 or HsKRAS4b. Scale bars: 100 μm. (B) Gametophore development defects of *ggb* are rescued by the YFP-PpROP4<sup>CVIM</sup> and YFP-AtROP1<sup>CVIM</sup>, although the rescued gametophores are substantially smaller. The plants were grown in BCDAT with 1 μM β-estradiol for 62 days. Scale bars:

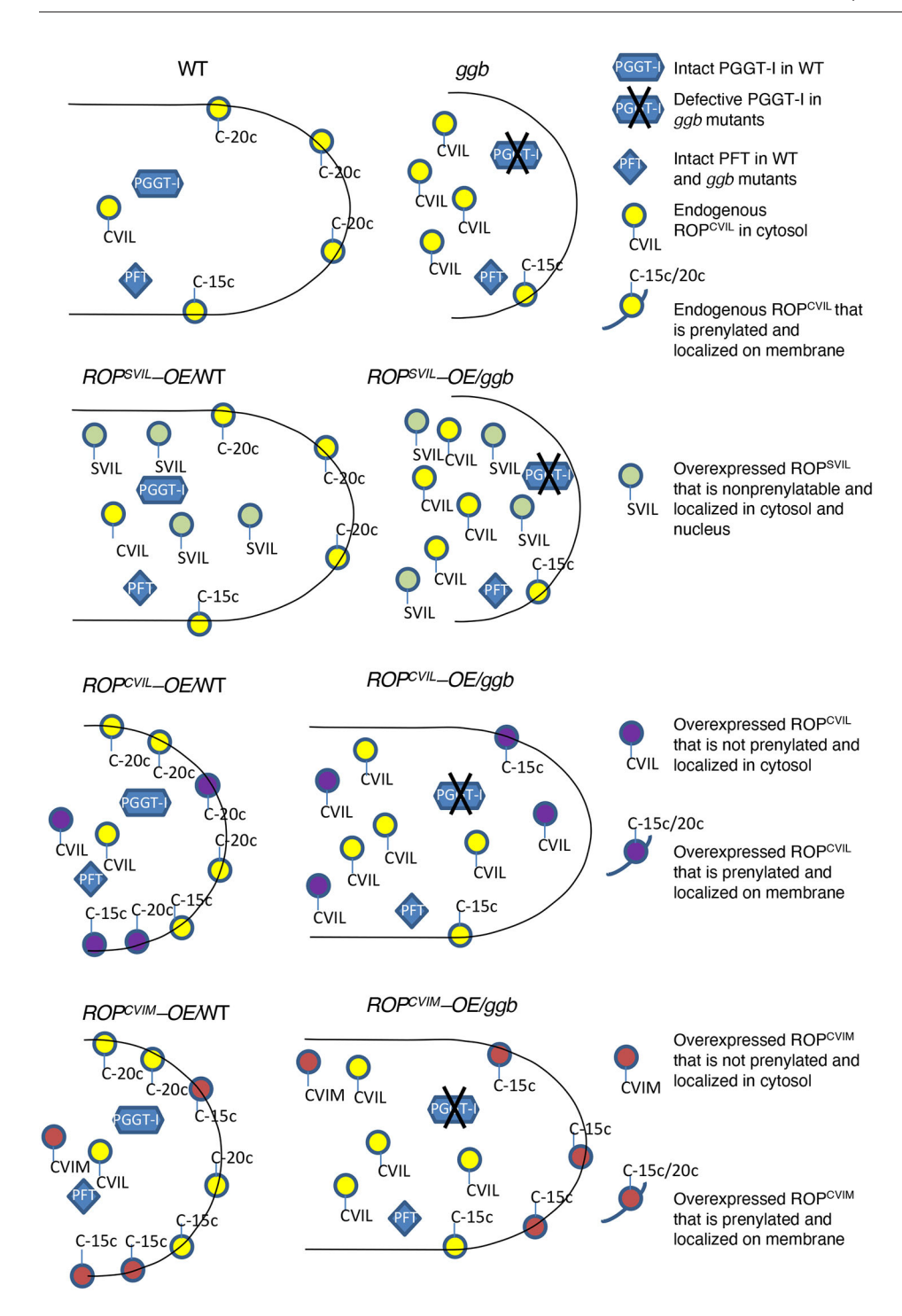


Fig. 5. Model for plant GGB/ROP regulation of multicellularity in the moss P. patens. In wild type, both PFT and PGGT-I are present, endogenous ROPCVIL may be prenylated by PFT and PGGT-I, and prenylation by PFT and PGGT-Lis responsible for cell adhesion, a prerequisite for tip growth and gametophore development. In ggb mutants where PGGT-I is absent, prenylation of endogenous ROPCVIL by PFT is not sufficient for multicellularity. In either wild type or ggb mutants, the nonprenylatable ROPSVIL cannot be lipid modified or located at the membrane and is inactive; thus, it does not have any effect on the cell morphology changes. In wild type, overexpressed ROPCVIL is mostly modified by PGGT-I, but some can be modified by PFT, and excess activated ROP induces cell expansion. In ggb mutants, overexpressed ROP<sup>CVIL</sup> that is prenylated by PFT is able to induce tip growth but not enough for gametophore development. In wild type, overexpressed ROP<sup>CVIM</sup> is mostly modified by PFT, but some can be modified by PGGT-I; excess activated ROP induces cell expansion. By contrast, in *ggb* mutants, overexpressed  $\mathsf{ROP}^\mathsf{CVIM}$  that is prenylated by PFT can induce both tip growth and gametophore development. 15c and 20c are farnesyl and geranylgeranyl isoprenoid groups, respectively.

superfamily. Interestingly, although *P. patens* and *Arabidopsis* have both PFT and PGGT-I, *P. patens* contains only ROPs with the CaaL motif, whereas *Arabidopsis* has ROPs with three different motifs: CaaL, CaaX and non CaaX/CaaL (Lavy et al., 2002). The *Arabidopsis* ROPs with CaaX or non CaaX/CaaL motifs are only palmitoylated by a different type of lipid modification from the prenylation (Lavy et al., 2002; Sorek et al., 2011). The present study suggests that, surprisingly, either PFT or PGGT-I of *P. patens* appears to be able to prenylate PpROP4. However, the activity of endogenous prenylated ROPs by PFT alone in the *ggb* mutant is not sufficient for multicellularity (Fig. 5). To compensate for the decreased ROP activity in *ggb* mutants, overexpressed ROPs that are terminated with CaaL are sufficient to induce tip growth but not for gametophore

development, while overexpressed ROPs with CaaX (CVIM in this case) are sufficient for both tip growth and gametophore development, probably because PFT more efficiently prenylates ROPs with CVIM than with CVIL. Therefore, we argue that the presence of ROPs with both CaaL and CaaX motifs may be advantageous in *Arabidopsis*, given that *ggb* deletion in *Arabidopsis* does not produce obvious developmental defects (Antimisiaris and Running, 2014).

#### MATERIALS AND METHODS

#### Subculture of P. patens

Protonemal tissue of wild-type and transgenic plants in the wild-type background was subcultured using a Polytron homogenizer T20B.S1 (IKA).

ggb mutants (Thole et al., 2014) and transgenic plants in the ggb mutant background were subcultured by pipetting with a P-1000 pipet in 5 ml autoclaved water. Homogenized tissue (2 ml) was spread and grown in each BCDAT agar medium (Nishiyama et al., 2000) in a 9 cm petri dish. Wild-type and transgenic plants in the wild-type background were grown in medium with cellophane, whereas ggb mutant and transgenic plants in the ggb mutant background were grown in medium without cellophane. Plants were grown at 25°C under continuous light at 50  $\mu$ mol m<sup>-2</sup> s<sup>-1</sup> intensity.

### Scanning electron microscopy and transmission electron microscopy

For scanning electron microscopy (SEM), plants were grown in BCDAT medium under white light for 6 days. The plants were then fixed with a fixative containing PME [100 mM PIPES, 5 mM EGTA, and 2 mM MgSO<sub>4</sub> (pH 6.8), 8% (w/v) paraformaldehyde, 1% (v/v) DMSO and 0.01% (v/v) Nonidet P-40] for1 h. Next, the samples were dehydrated through a graded series of ethanol (10%, 20%, 40%, 80% and 100%, once for 10 min at each step), then kept in 100% ethanol. After drying at critical point (Tousimis 815A critical point dryer) using liquefied carbon dioxide as the transitional fluid, the samples were sputter coated with gold. A Zeiss EVO 40 scanning electron microscope was used for visualization with a smartSEM software at 3.0 KV.

For TEM, plants were embedded within BCDATG medium supplemented with 0.5% glucose and 0.4% gellan gum, and cultured for 6 days under white light. For transmission electron microscopy (TEM) they were processed following the protocol of Pressel et al. (2008). Briefly, the tissues were fixed in 3% (v/v) glutaraldehyde, 1% (v/v) formaldehyde (freshly prepared from paraformaldehyde) and 0.5% (w/v) tannic acid in 0.05 M sodium phosphate buffer (pH 7.0) for 3 h at room temperature. After rinsing in 0.1 M sodium phosphate buffer, the material was post-fixed with 1% (w/v) osmium tetroxide in 0.1 M sodium phosphate buffer (pH 6.8) overnight at 4°C, dehydrated through an ethanol series as above and embedded in Embed812 resin via propylene oxide (Electron Microscopy Sciences). Ultrathin sections (60 nm) were cut using a diamond knife and were sequentially stained with 8% (v/v) methanolic uranyl acetate for 30 min and lead citrate for 2 min, and the sections were examined with an HT7700 electron microscope (Hitachi).

#### **Microsphere experiments**

The microsphere experiments followed the previous protocol of Menand et al. (2007). Wild-type protonema was grown in unilateral red light (to allow the linear protonemal cells to align so that the cells would be in a similar focus plane for confocal imaging) or ggb under white light (ggb mutants did not grow sufficiently under unilateral red light). The FluoSpheres sulphate microspheres, 0.2 µm, yellow-green fluorescent (F8848, Invitrogen) were washed five times in water before use. Seven-day-old plants were incubated for 5 min in 10  $\mu$ l of 0.2% microspheres in the BCDATG liquid medium and then for 2 min in 10 µl calcofluor white, and, after the staining, the plants were washed in 3 ml of BCDATG liquid medium once. The wild-type protonemal tissue was cultured in liquid BCDATG medium. For ggb mutants, the cells were embedded within BCDATG solid medium (ggb cells are too motile in a liquid medium). Wild-type and ggb mutants were irradiated with white light that is provided by the transmission light of the microscope from above during imaging. A Nikon A1 confocal microscope with NIS element software was used for imaging with the 418 nm laser for calcoflour visualization and the 488 nm laser for microsphere visualization. For both calcofluor white and microspheres, the images were taken with the pinhole at 1.0, HV-gain at 100, offset-background adjustment at 0, a scan size at 1024×1024 and a scan speed at 1/2 frame per second. Laser power at 5% to 7% was used for calcofluor white and 0.3% to 1% for microsphere. The time interval between each data acquisition period was 6 h for wild-type protonemal cells and 24 h for ggb mutants.

#### 3-D image re-construction

Calcofluor white (Sigma-Aldrich, 18909-100ML-F) was sterilized with a 0.22  $\mu$ m filter and stored at 4°C before use. *ggb* mutant plants were dispersed in 20  $\mu$ l of sterilized water and mixed with 10  $\mu$ l of the sterilized calcofluor white for 2 min. The plants were then mixed with 200  $\mu$ l of

cooled BCDATG, containing BCDAT medium supplemented with 0.5%glucose and 0.4% gellan gum (Nacalai Tesque, 12389-96). After mixing, all of the mixture was transferred into a 27 mm diameter glass base dish (Iwaki, 3930-035). After solidifying, the mixture was covered with 3 ml of cooled BCDATG and set for 10 min for solidifying again. On the bottom of the dish, 10 lines were then drawn horizontal and vertical directions to mark the positions. The plants were grown for 7 days under red light (about  $2 \mu \text{mol m}^{-2} \text{ s}^{-1}$ ) with the dish inverted. The red-light environment was provided by passing light through a 3-mm red plastic filter (Mitsubishi). Before imaging, the plants were precultured under white light for 2 days before being subjected to time-lapse imaging every day. A Nikon A1 confocal microscope with NIS element software was used for visualization of calcofluor with the 418 nm laser. The images were taken with the pinhole at 1.0, HV-gain at 100, offset-background adjustment at 0, laser power at 5% to 7%, a scan size at 1024×1024 and scan speed at 1/2 frame per second. Seventeen to 22 z-series optical sections were collected with a step size of 1.0 µm. NIS elements software was used for construct 3-D images.

#### **Transformation**

Polyethylene glycol-mediated transformation of *Physcomitrium* protoplasts was performed following standard procedures (Ito et al., 2014). Briefly, moss protoplasts were mixed with MMM solution, linearized plasmid DNA and PEG solution, and heat shocked at 45°C for 5 min followed by incubation at 20°C for 10 min. After washing with 8% mannitol, the protoplasts were mixed with PRM/T and spread onto PRM/B medium for regeneration for 10 days. The regenerated plants were then transferred onto BCDAT selection medium with 30  $\mu$ g/l hygromycin (Invitrogen) or 100  $\mu$ g/l zeocin (Alfa Aesar). The selection lasted 10 days and was followed by a 7-day release period on BCDAT without antibiotic. A second selection was then conducted after the release. Plants surviving the second round of selection were screened by PCR or by fluorescence microscopy.

#### **Immunostaining**

Protonemata of wild-type and cells of ggb mutants were grown on BCDAT medium, and cells of amiRNA-ROP plants were grown in BCDAT supplemented with 1 μM β-estradiol for 7 days. The immunostaining experiment follows the procedures of Hiwatashi (Hiwatashi et al., 2014). Briefly, cells were fixed in PME solution [100 mM PIPES, 5 mM EGTA and 2 mM MgSO<sub>4</sub> (pH 6.8)] with 8% (w/v) paraformaldehyde, 1% (v/v) DMSO and 0.01% (v/v) Nonidet P-40 for 1 h. The samples were then washed in PMEN0.01 [PME supplemented with 0.01% (v/v) Nonidet P-40] and attached to cover glasses that were coated with 0.1% polyethylene-imine. The attached cells were treated with a driselase solution [2% (w/v) driselase, 0.4 M mannitol and 1× proteinase inhibitor (Roche)] for 10 min at room temperature. Cells were then washed with PMEN0.01 three times and soaked in ice-cold methanol for 10 min at -20°C. After washing with PMEN0.01, samples were blocked with a solution containing 0.05% (v/v) Triton X-100 and 0.05% (w/v) BSA for 10 min. Later, cells were washed with PBS and incubated with mouse anti-α-tubulin monoclonal antibody (Sigma-Aldrich) at dilution of 1:100 in PBS overnight at 4°C. Cells were then treated with Alexa Fluor 546 goat anti-mouse IgG (Invitrogen) for 3 h at 37°C. After rinsing with PBS, cells were stained with 0.2 mg/l DAPI for 10 min. After washing with PBS, the cells were mounted with a ProLong Gold Antifade Mountant (Themo Fisher Scientific). For quantification of the orientation of microtubules, angles were measured at 2 µm from the plus or minus ends. For measuring angles, ImageJ was used (https://imagej.nih.gov/ij/).

#### **Plasmid construction**

The primers used for in this study are listed in Table S1. The design of amiRNAs followed Khraiwesh et al. (2008). Ideal miRNA target sites for the four *P. patens* ROPs were identified using Web MicroRNA Designer (http://wmd3.weigelworld.org/). The ROP-amiRNA sequences were obtained by using the *Arabidopsis* (*Arabidopsis thaliana*) miR319a precursor pRS300 as a template for overlapping PCR (Schwab et al., 2006). The resultant PCR fragment was cloned into pENTR/D-TOPO (Invitrogen, K240020) and introduced into the destination vector PGX8 (Kubo et al., 2013) to construct PGX8-ROP-amiRNA plasmids by the LR reaction using LR clonase II (Invitrogen, 11791020).

To construct pCAM-PpROP4-YFP, the open reading frame of PpROP4 was amplified by PCR and the PpROP was cloned to pCAM-YFP with restriction enzymes BgIII and KpnI. YFP-PpROP4<sup>CVIL</sup>, YFP-ROP4<sup>CVIM</sup> and YFP-PpROP4<sup>SVIIL</sup> were amplified by using pCAM-YFP-PpROP4 as a template, and the CVIL, CVIM and SVIL point mutations at the C-terminal were introduced by using a corresponding reverse primer (Table S1). To construct PGX8-YFP-PpROP4<sup>CVIL</sup>, PGX8-YFP-PpROP4<sup>CVIM</sup> and PGX8-YFP-PpROP4<sup>SVIL</sup>, the resultant PCR fragments were cloned into pENTR/D-TOPO and introduced into the destination vector PGX8.

The AtROP1<sup>CVIM</sup>, HsRAC1<sup>CVIM</sup> and HsKRAS4b<sup>CVIM</sup> were amplified by PCR from plasmids of ECFP-AtROP1 (Gu et al., 2005), YFP-Rac1 (Hoppe and Swanson, 2004) (a gift from Joel Swanson, University of Michigan Medical School, USA; Addgene plasmid #11391) and pcDNA3.1-YFP-KRAS4B (a gift from Kenneth Westover, UT Southwestern Medical Center, USA; Addgene plasmid #112718), respectively. The YPF was amplified from pCAM-PpROP4-YFP with corresponding primers (Table S1). AtROP1, HsRAC1 or HsKRAS4b was mixed with corresponding YFP at ratio of 1:1. The mixture was used as templates to amplify YFP-AtROP1<sup>CVIM</sup>, YFP-HsRAC1<sup>CVIM</sup> and YFP-HsKRAS4b<sup>CVIM</sup>. To construct PGX8-YFP-AtROP1<sup>CVIM</sup>, PGX8-YFP-HsRAC1<sup>CVIM</sup> and PGX8-YFP-HsKRAS4b<sup>CVIM</sup>, the resultant PCR fragments were cloned into pENTR/D-TOPO and introduced to PGX8.

To construct the vector for expressing YFP-AtRabA4d in moss, YFP-AtRabA4d was amplified by PCR using 35S:eYFP-AtRabA4d (a gift from Dr E. Nielsen, University of Michigan, USA) as a template. The resultant PCR fragment were cloned into pENTR/D-TOPO and introduced into the destination vector pT1OG (Aoyama et al., 2012) to construct T1OG-YFP-AtRabA4d by LR reaction.

#### **RNA** extraction and RT-PCR

For qPCR analysis of the expression of the four PpROP genes, homogenized PGX8-amiRNA-ROP plants were grown in BCDAT supplemented with 1  $\mu$ M  $\beta$ -estradiol and wild-type in BCDAT for 7 days. Approximately 100 mg of tissue was ground in liquid nitrogen, and total RNA was extracted with the RNeasy plant mini kit (Qiagen, 74904) and treated with RNase-free DNase I (Qiagen, 79254) to remove genomic DNA. 0.5 µg of total RNA was reverse transcribed using the ImProm-II Reverse Transcription System (Promega, A3800) in a 20 µl RT first-strand synthesis reaction that contained oligo(dT) primers. The reverse transcription reaction was subsequently diluted to 20× with RNase-free water, and 1 µl of 20× diluted cDNA was used as a template in a 20 µl reaction using the SYBR green master mix (Invitrogen, A25741). The PCR conditions were as follows: 95°C for 10 min, followed by 40 cycles of 95°C for 30 s and 60°C for 1 min, and ending with a melting curve analysis. Design of the qPCR primers (Table S1) of four ROPs and endogenous control Ubi10 follows a previous study (Burkart et al., 2015). Amplification efficiencies were used in the calculation of the relative expression levels.

#### **Polartropism analysis**

To examine directional growth, the protoplasts were isolated and regenerated in PRM/B medium (Ito et al., 2014) in a petri dish with the lid replaced by a glass cover and grown under polarized white light that is generated by passing the light through a polarizer (HN32; Sumitomo 3 M) in a light-proof box. The plants were grown under continuous light at 25°C for 27 days and imaged using a Nikon TE200 microscope equipped with a DS-U3 camera.

#### **Accession numbers**

AtROP1 mRNA sequence (NM\_114989), HsRAC1 protein sequence (NP\_008839) and HsKRAS4b protein sequence (NP\_004976) can be found in GenBank, and PpROP1 (Pp3c14\_4310), PpROP2 (Pp3c2\_20700), PpROP3 (Pp3c1\_21550) and PpROP4 (Pp3c10\_4950) gene loci in Phytozome.

#### Acknowledgements

The authors thank Dr Evgeniya Moiseeva at the Micro/Nano Technology Center, University of Louisville and Dr Tanya E. S. Dahms at the University of Regina for assistance with SEM, and Dr Soucy Patricia and Betty Nunn at University of Louisville for assistance with confocal microscope. We thank Dr Hasebe Mistuyasu

of NIBB for providing PGX8 and T1OG vectors, Dr Detlef Weigel for the pRS300 plasmid, Dr Zhengbiao Yang of the University of California (Riverside) for ECFP-AtROP1 plasmid and Dr Erik Nielsen of the University of Michigan for the 35s:eYFP-RabA4d plasmid. We also thank Dr Liam Dolan at the University of Oxford and Dr. Benoît Menand at Bioscience and Biotechnology Institute of Aix-Marseille for assistance of microsphere experiment.

#### Competing interests

The authors declare no competing or financial interests.

#### **Author contributions**

Conceptualization: L.B., T.F., M.P.R.; Methodology: L.B., J.R., M.N., A.S.S., J.M.T., M.P.R.; Software: L.B.; Validation: L.B., M.P.R.; Formal analysis: L.B.; Investigation: L.B., J.R., M.P.R.; Resources: M.P.R.; Data curation: L.B., J.R., M.P.R.; Writing original draft: L.B.; Writing - review & editing: L.B., J.R., M.N., A.S.S., J.M.T., S.P.M., J.H., T.F., M.P.R.; Visualization: L.B., J.R., M.N., A.S.S., S.P.M.; Supervision: L.B., M.P.R.; Project administration: L.B., T.F., M.P.R.; Funding acquisition: M.P.R.

#### **Funding**

This work was funded in part by the National Science Foundation (1456884 to M.P.R.) and by a National Science Foundation Cooperative Agreement (1849213 to M.P.R.).

#### Peer review history

The peer review history is available online at https://journals.biologists.com/dev/article-lookup/doi/10.1242/dev.200279.

#### References

- **Abedin, M. and King, N.** (2010). Diverse evolutionary paths to cell adhesion. *Trends Cell Biol.* **20**, 734-742. doi:10.1016/j.tcb.2010.08.002
- Antimisiaris, M. F. and Running, M. P. (2014). Turning moss into algae: Prenylation targets in *Physcomitrella patens*. *Plant Signal*. *Behav.* 9, 7. doi:10. 4161/psb.29314
- Aoyama, T., Hiwatashi, Y., Shigyo, M., Kofuji, R., Kubo, M., Ito, M. and Hasebe, M. (2012). AP2-type transcription factors determine stem cell identity in the moss *Physcomitrella patens*. *Development* 139, 3120-3129. doi:10.1242/dev.076091
- Brunet, T. and King, N. (2017). The origin of animal multicellularity and cell differentiation. *Dev. Cell* 43, 124-140. doi:10.1016/j.devcel.2017.09.016
- Burkart, G. M., Baskin, T. I. and Bezanilla, M. (2015). A family of ROP proteins that suppresses actin dynamics, and is essential for polarized growth and cell adhesion. J. Cell Sci. 128, 2553-2564. doi:10.1242/jcs.172445
- Cavalier-Smith, T. (2017). Origin of animal multicellularity: precursors, causes, consequences-the choanoflagellate/sponge transition, neurogenesis and the Cambrian explosion. *Philos. Trans. R. Soc. Lond. B Biol. Sci.* 372, 20150476. doi:10.1098/rstb.2015.0476
- Cheng, X., Mwaura, B. W., Chang Stauffer, S. R. and Bezanilla, M. (2020). A fully functional ROP fluorescent fusion protein reveals roles for this GTPase in subcellular and tissue-level patterning. *Plant Cell* 32, 3436-3451. doi:10.1105/tpc. 20.00440
- Cove, D., Bezanilla, M., Harries, P. and Quatrano, R. (2006). Mosses as model systems for the study of metabolism and development. *Annu. Rev. Plant Biol.* 57, 497-520. doi:10.1146/annurev.arplant.57.032905.105338
- Crowell, D. N. and Huizinga, D. H. (2009). Protein isoprenylation: the fat of the matter. *Trends Plant Sci.* 14, 163-170. doi:10.1016/j.tplants.2008.12.001
- Eklund, D. M., Svensson, E. M. and Kost, B. (2010). *Physcomitrella patens*: a model to investigate the role of RAC/ROP GTPase signalling in tip growth. *J. Exp. Bot.* **61**, 1917-1937. doi:10.1093/jxb/erq080
- Galichet, A. and Gruissem, W. (2006). Developmentally controlled farnesylation modulates AtNAP1;1 function in cell proliferation and cell expansion during Arabidopsis leaf development. *Plant Physiol.* 142, 1412-1426. doi:10.1104/pp. 106.088344
- Gu, Y., Fu, Y., Dowd, P., Li, S., Vernoud, V., Gilroy, S. and Yang, Z. (2005). A Rho family GTPase controls actin dynamics and tip growth via two counteracting downstream pathways in pollen tubes. *J. Cell Biol.* 169, 127-138. doi:10.1083/jcb. 200409140
- Heaton, L. L. M., Jones, N. S. and Fricker, M. D. (2020). A mechanistic explanation of the transition to simple multicellularity in fungi. *Nat. Commun.* 11, 2594. doi:10. 1038/s41467-020-16072-4
- Hiwatashi, Y., Sato, Y. and Doonan, J. H. (2014). Kinesins have a dual function in organizing microtubules during both tip growth and cytokinesis in *Physcomitrella* patens. Plant Cell 26, 1256-1266. doi:10.1105/tpc.113.121723
- Holmes, D. L., Lancaster, A. K., Lindquist, S. and Halfmann, R. (2013). Heritable remodeling of yeast multicellularity by an environmentally responsive prion. *Cell* 153, 153-165. doi:10.1016/j.cell.2013.02.026
- Hoppe, A. D. and Swanson, J. A. (2004). Cdc42, Rac1, and Rac2 display distinct patterns of activation during phagocytosis. *Mol. Biol. Cell* 15, 3509-3519. doi:10. 1091/mbc.e03-11-0847

- Ito, K., Ren, J. and Fujita, T. (2014). Conserved function of Rho-related Rop/RAC GTPase signaling in regulation of cell polarity in *Physicomitrella patens*. Gene 544, 241-247. doi:10.1016/j.gene.2014.04.057
- Jarvis, M. C., Briggs, S. P. H. and Knox, J. P. (2003). Intercellular adhesion and cell separation in plants. *Plant Cell Environ.* 26, 977-989. doi:10.1046/j.1365-3040.2003.01034.x
- **Jenkins, G. I. and Cove, D. J.** (1983). Phototropism and polarotropism of primary chloronemata of the moss *Physcomitrella patens*: responses of the wild-type. *Planta* **158**, 357-364. doi:10.1007/BF00397338
- Johnson, C. D., Chary, S. N., Chernoff, E. A., Zeng, Q., Running, M. P. and Crowell, D. N. (2005). Protein geranylgeranyltransferase I is involved in specific aspects of abscisic acid and auxin signaling in *Arabidopsis*. *Plant Physiol.* 139, 722-733. doi:10.1104/pp.105.065045
- Kawabe, Y., Du, Q., Schilde, C. and Schaap, P. (2019). Evolution of multicellularity in Dictyostelia. *Int. J. Dev. Biol.* 63, 359-369. doi:10.1387/ijdb.190108ps
- Khraiwesh, B., Ossowski, S., Weigel, D., Reski, R. and Frank, W. (2008). Specific gene silencing by artificial MicroRNAs in *Physcomitrella patens*: an alternative to targeted gene knockouts. *Plant Physiol.* 148, 684-693. doi:10.1104/pp.108. 128025
- Knoll, A. H. (2011). The multiple origins of complex multicellularity. Annu. Rev. Earth Planet. Sci. 39, 217-239. doi:10.1146/annurev.earth.031208.100209
- Kubo, M., Imai, A., Nishiyama, T., Ishikawa, M., Sato, Y., Kurata, T., Hiwatashi, Y., Reski, R. and Hasebe, M. (2013). System for stable β-estradiol-inducible gene expression in the moss *Physcomitrella patens*. *PLos ONE* 8, e77356. doi:10. 1371/journal.pone.0077356
- Lavy, M., Bracha-Drori, K., Sternberg, H. and Yalovsky, S. (2002). A cell-specific, prenylation-independent mechanism regulates targeting of type II RACs. *Plant Cell* 14, 2431-2450. doi:10.1105/tpc.005561
- McCormack, J., Welsh, N. J. and Braga, V. M. M. (2013). Cycling around cell-cell adhesion with Rho GTPase regulators. *J. Cell Sci.* **126**, 379-391. doi:10.1242/jcs. 097923
- Menand, B., Calder, G. and Dolan, L. (2007). Both chloronemal and caulonemal cells expand by tip growth in the moss *Physcomitrella patens*. *J. Exp. Bot.* 58, 1843-1849. doi:10.1093/jxb/erm047
- Moody, L. A. (2019). The 2D to 3D growth transition in the moss Physcomitrella patens. Curr. Opin. Plant Biol. 47, 88-95. doi:10.1016/j.pbi.2018.10.001
- Moody, L. A., Kelly, S., Clayton, R., Weeks, Z., Emms, D. M. and Langdale, J. A. (2021). NO GAMETOPHORES 2 Is a Novel Regulator of the 2D to 3D Growth Transition in the Moss Physcomitrella patens. *Curr. Biol.* 31, 555-563.e54. doi:10.1016/j.cub.2020.10.077
- Niklas, K. J. (2014). The evolutionary-developmental origins of multicellularity. Am. J. Bot. 101, 6-25. doi:10.3732/ajb.1300314
- Niklas, K. J. and Newman, S. A. (2020). The many roads to and from multicellularity. *J. Exp. Bot.* **71**, 3247-3253. doi:10.1093/jxb/erz547
- Nishiyama, T., Hiwatashi, Y., Sakakibara, K., Kato, M. and Hasebe, M. (2000). Tagged mutagenesis and gene-trap in the moss, *Physcomitrella patens* by shuttle mutagenesis. *DNA Res.* 7, 9-17. doi:10.1093/dnares/7.1.9
- Pentz, J. T., Márquez-Zacarías, P., Bozdag, G. O., Burnetti, A., Yunker, P. J., Libby, E. and Ratcliff, W. C. (2020). Ecological advantages and evolutionary limitations of aggregative multicellular development. *Curr. Biol.* 30, 4155-4164.e56. doi:10.1016/j.cub.2020.08.006
- Perroud, P.-F. and Quatrano, R. S. (2008). BRICK1 is required for apical cell growth in filaments of the moss Physcomitrella patens but not for gametophore morphology. Plant Cell 20, 411-422. doi:10.1105/tpc.107.053256

- Pressel, S., Ligrone, R. and Duckett, J. G. (2008). Cellular differentiation in moss protonemata: a morphological and experimental study. *Ann. Bot.* 102, 227-245. doi:10.1093/aob/mcn080
- Prochnik, S. E., Umen, J., Nedelcu, A. M., Hallmann, A., Miller, S. M., Nishii, I., Ferris, P., Kuo, A., Mitros, T., Fritz-Laylin, L. K. et al. (2010). Genomic analysis of organismal complexity in the multicellular green alga Volvox carteri. Science 329, 223-226. doi:10.1126/science.1188800
- Ratcliff, W. C., Herron, M. D., Howell, K., Pentz, J. T., Rosenzweig, F. and Travisano, M. (2013). Experimental evolution of an alternating uni- and multicellular life cycle in *Chlamydomonas reinhardtii*. *Nat. Commun.* **4**, 2742. doi:10.1038/ncomms3742
- Rojas, A. M., Fuentes, G., Rausell, A. and Valencia, A. (2012). The Ras protein superfamily: evolutionary tree and role of conserved amino acids. *J. Cell Biol.* 196, 189-201. doi:10.1083/jcb.201103008
- Rokas, A. (2008). The molecular origins of multicellular transitions. *Curr. Opin. Genet. Dev.* **18**, 472-478. doi:10.1016/j.gde.2008.09.004
- Rozario, T. and DeSimone, D. W. (2010). The extracellular matrix in development and morphogenesis: a dynamic view. *Dev. Biol.* 341, 126-140. doi:10.1016/j. ydbio.2009.10.026
- Running, M. P. (2014). The role of lipid post–translational modification in plant developmental processes. Front. Plant Sci. 5, 50. doi:10.3389/fpls.2014.00050
- Running, M. P., Lavy, M., Sternberg, H., Galichet, A., Gruissem, W., Hake, S., Ori, N. and Yalovsky, S. (2004). Enlarged meristems and delayed growth in plp mutants result from lack of CaaX prenyltransferases. *Proc. Natl. Acad. Sci. USA* 101, 7815-7820. doi:10.1073/pnas.0402385101
- Schwab, R., Ossowski, S., Riester, M., Warthmann, N. and Weigel, D. (2006). Highly specific gene silencing by artificial microRNAs in *Arabidopsis. Plant Cell* **18**, 1121-1133. doi:10.1105/tpc.105.039834
- Seymour, G. B., Tucker, G. and Leach, L. A. (2004). Cell adhesion molecules in plants and animals. *Biotechnol. Genet. Eng. Rev.* 21, 123-132. doi:10.1080/ 02648725.2004.10648051
- Smith, L. G. (2001). Plant cell division: building walls in the right places. Nat. Rev. Mol. Cell Biol. 2, 33-39. doi:10.1038/35048050
- Sorek, N., Gutman, O., Bar, E., Abu-Abied, M., Feng, X., Running, M. P., Lewinsohn, E., Ori, N., Sadot, E., Henis, Y. I. et al. (2011). Differential effects of prenylation and s-acylation on type I and II ROPS membrane interaction and function. *Plant Physiol.* 155, 706-720. doi:10.1104/pp.110.166850
- Tang, H., Duijts, K., Bezanilla, M., Scheres, B., Vermeer, J. E. M. and Willemsen, V. (2020). Geometric cues forecast the switch from two– to three– dimensional growth in *Physcomitrella patens*. New Phytol. 225, 1945-1955. doi:10.1111/nph. 16276
- Thole, J. M., Perroud, P.-F., Quatrano, R. S. and Running, M. P. (2014).
  Prenylation is required for polar cell elongation, cell adhesion, and differentiation in *Physcomitrella patens*. *Plant J.* 78, 441-451. doi:10.1111/tpj.12484
- Whitewoods, C. D., Cammarata, J., Nemec Venza, Z., Sang, S., Crook, A. D., Aoyama, T., Wang, X. Y., Waller, M., Kamisugi, Y., Cuming, A. C. et al. (2018). CLAVATA was a genetic novelty for the morphological innovation of 3D growth in land plants. *Curr. Biol.* 28, 2365-2376.e65. doi:10.1016/j.cub.2018.05.068
- Yalovsky, S. (2015). Protein lipid modifications and the regulation of ROP GTPase function. *J. Exp. Bot.* **66**, 1617-1624. doi:10.1093/jxb/erv057
- Yi, P. and Goshima, G. (2020). Rho of Plants GTPases and cytoskeletal elements control nuclear positioning and asymmetric cell division during *Physcomitrella* patens branching. Curr. Biol. 30, 2860-2868.e63. doi:10.1016/j.cub.2020.05.022

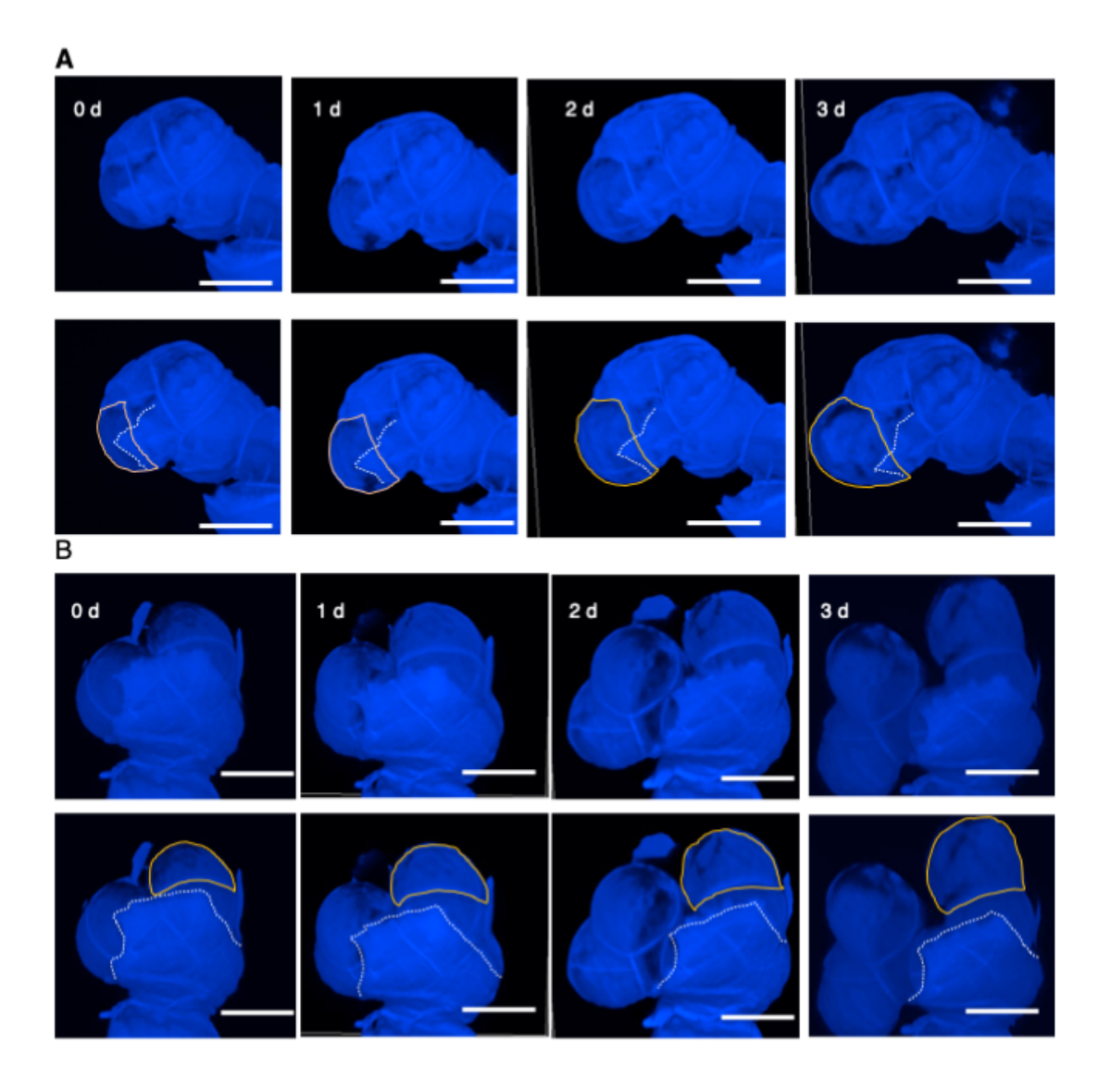


**Fig. S1.** 3-D time series (three days in total) showing the development of ggb. Two plants are shown for early (**A**) and later (**B**) development of cell separation. Note that, the area of cell wall surface covering the cell was gradually decreased from day 0 to day 3. White dash lines below each image indicate the broken surface cell walls on the expanding cells, and orange lines indicate the cells beneath the cell wall surface in ggb. Scale bar: 20  $\mu$ m.

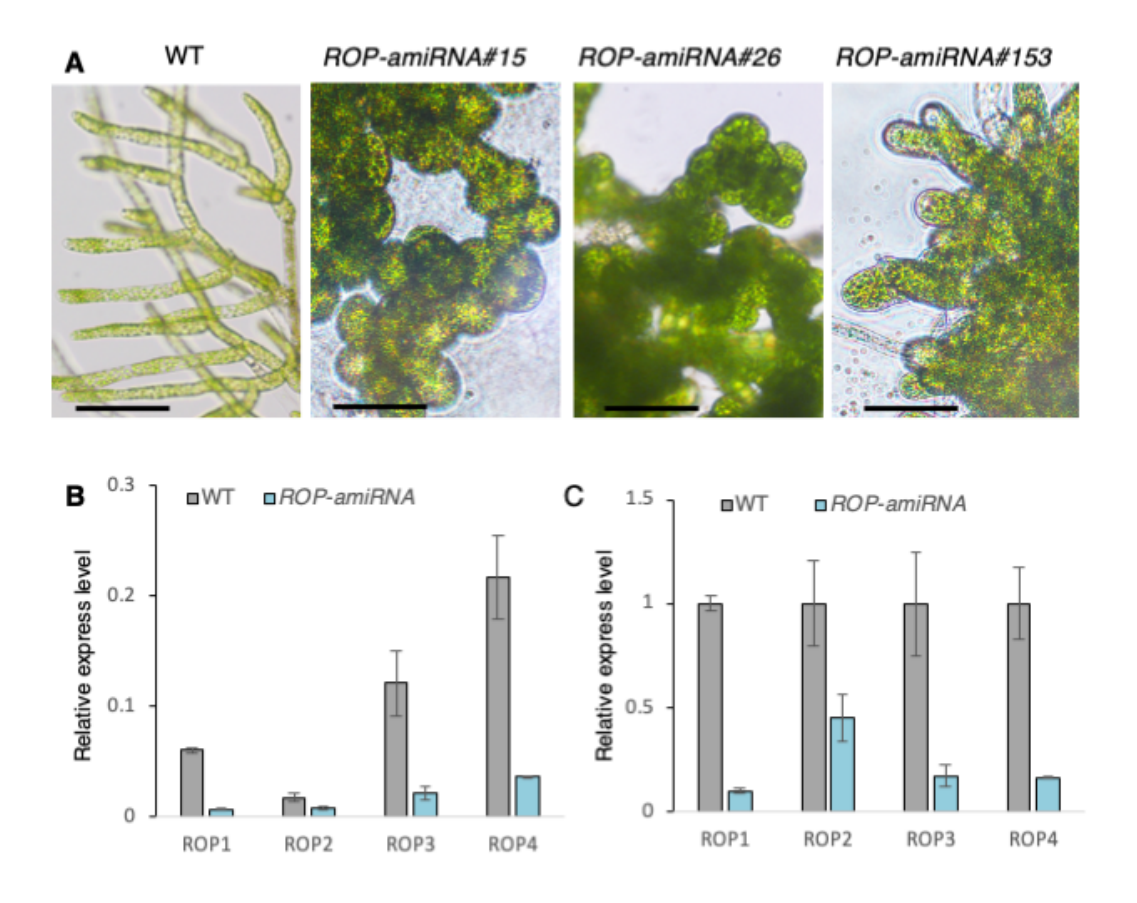
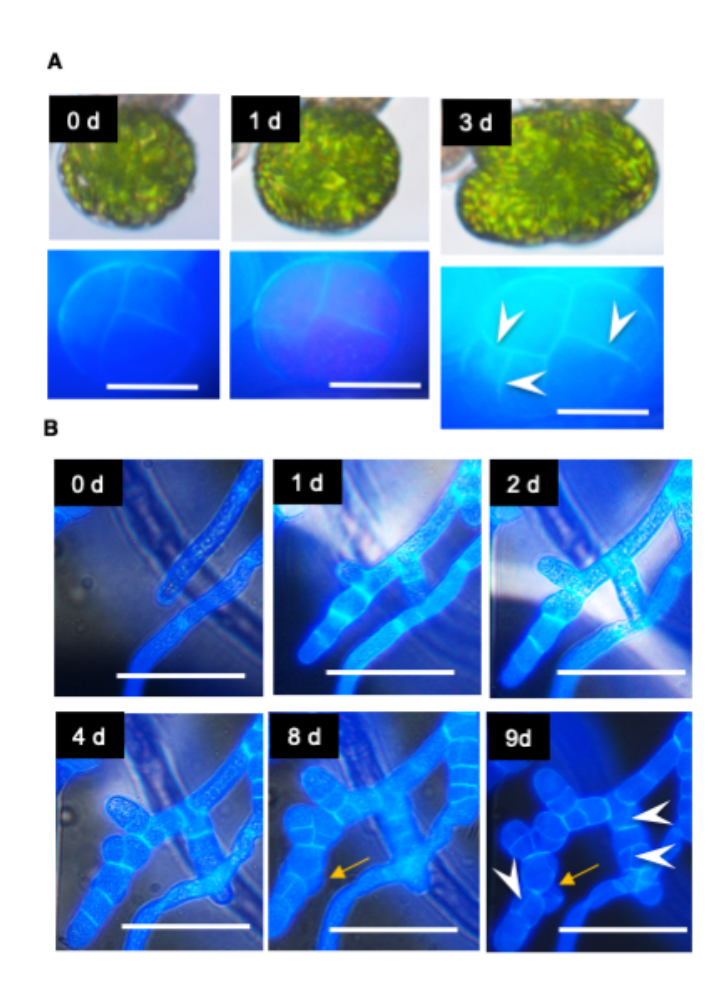


Fig. S2. Expression levels of *PpROPs* in WT and *ROP-amiRNA*.

**A**, Inhibition of cell elongation in different *ROP-amiRNA* lines #15, #26 and #153. The different *ROP-amiRNA* lines were grown in BCDAT supplemented with  $1\mu$ M  $\beta$ -estradiol for two weeks.

Scale bar: 100 μm. **B**, Relative expression (normalized to Ubi10) of *PpROP* genes in 7-day-old WT grown in BCDAT and *ROP-amiRNA* in BCDAT supplemented with 1μM β-estradiol. **C**, Relative expression levels in *ROP-amiRNA* plant, normalized to that in wild type.



**Fig. S3. Defect of cell plate orientation in** *ggb* **mutants and** *ROP-amiRNA* **plants.** Live imaging of *ggb* mutants for 3 days (**A**) and *ROP-amiRNA#26* induced by 1  $\mu$ M  $\beta$ -estradiol for 9 days (**B**). Note that cell separation occurred on 8 days after inducible knockdown (yellow arrows). Arrow heads show randomized cell division orientation that were shown in last day. Scale bar:20  $\mu$ m (**A**) and 100  $\mu$ m (**B**).

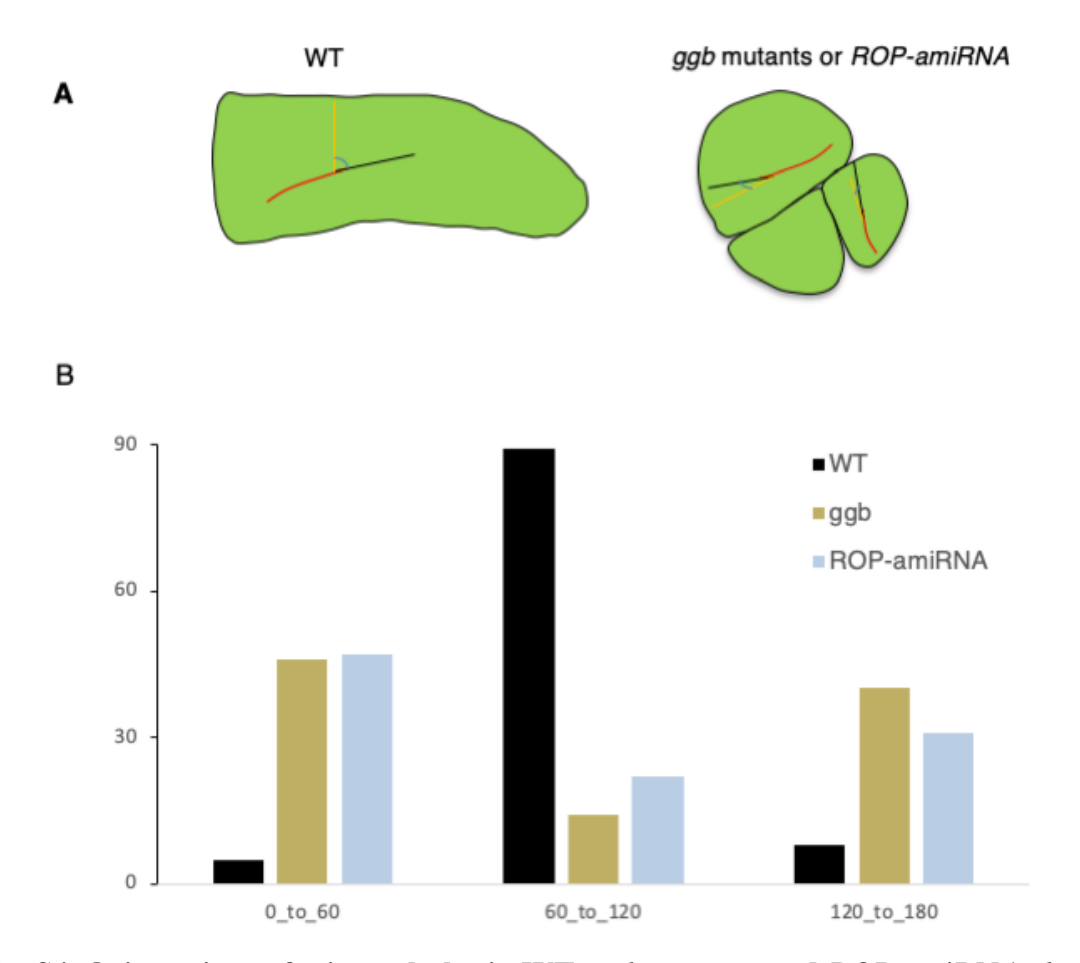
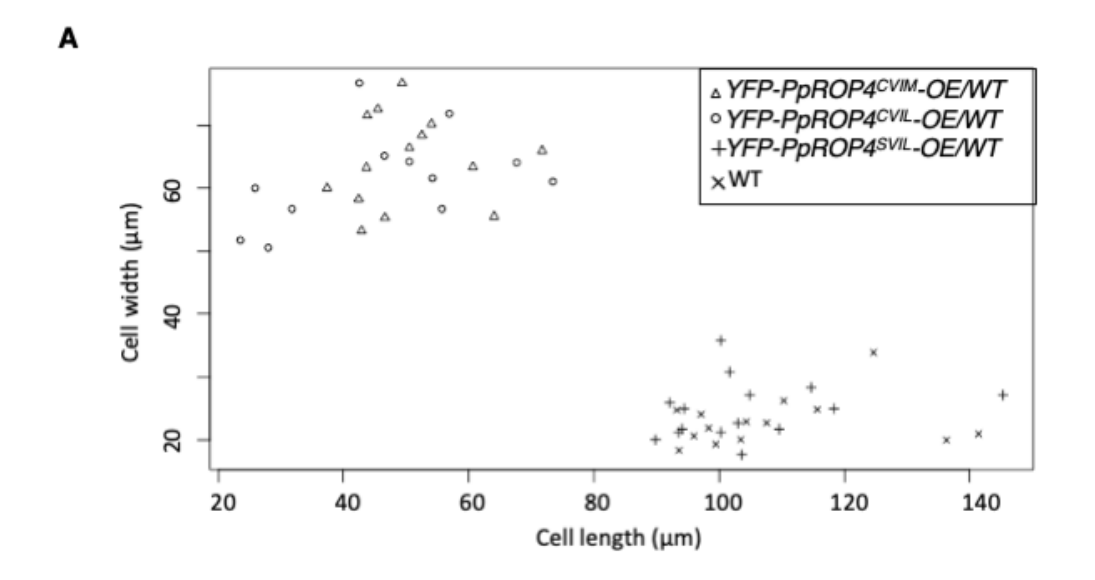


Fig. S4. Orientations of microtubules in WT, ggb mutants and ROP-amiRNA plants

A, Schematic illustration about the methods for measuring orientation of microtubules. Angles are measured at 2 µm from the plus ends or minus ends against the cross wall of the newly formed cross wall. B, Distributions of microtubule angles of three categories, from 0 to 60 degrees, 60 to 120 degrees and 120 to 180 degrees. Plus or minus ends of 100 microtubules from three cells in WT, *ggb* mutants and *ROP-amiRNA* plants were randomly selected for the measurements.



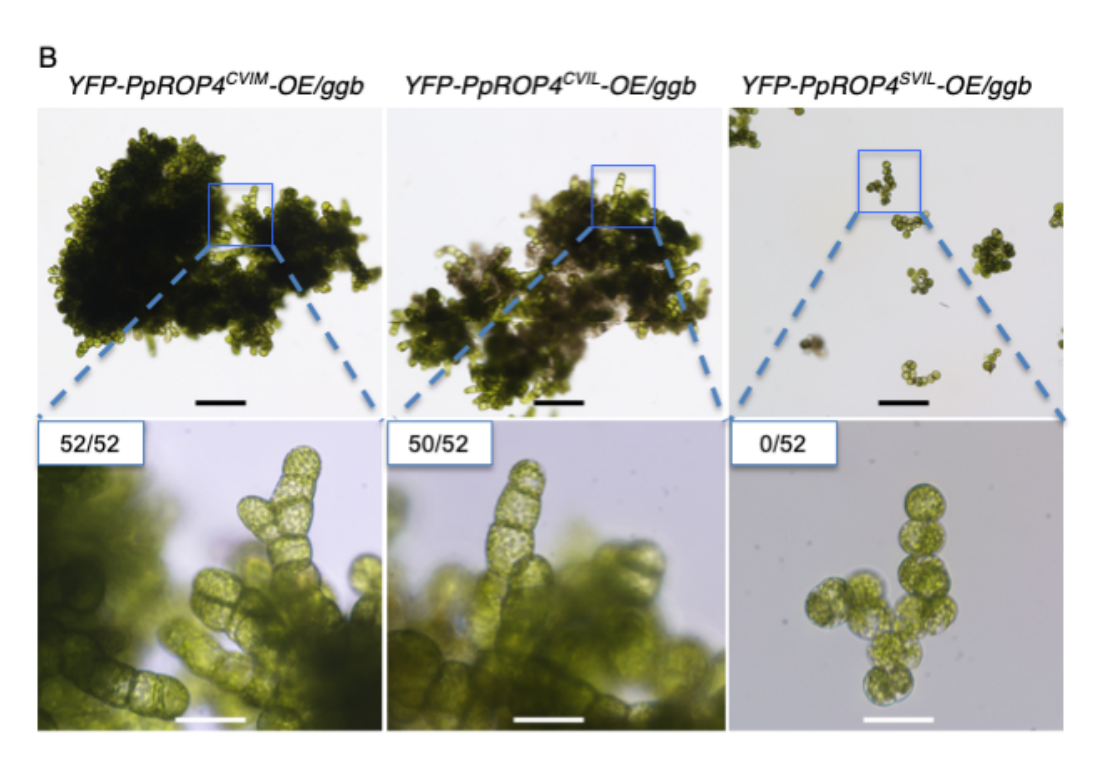
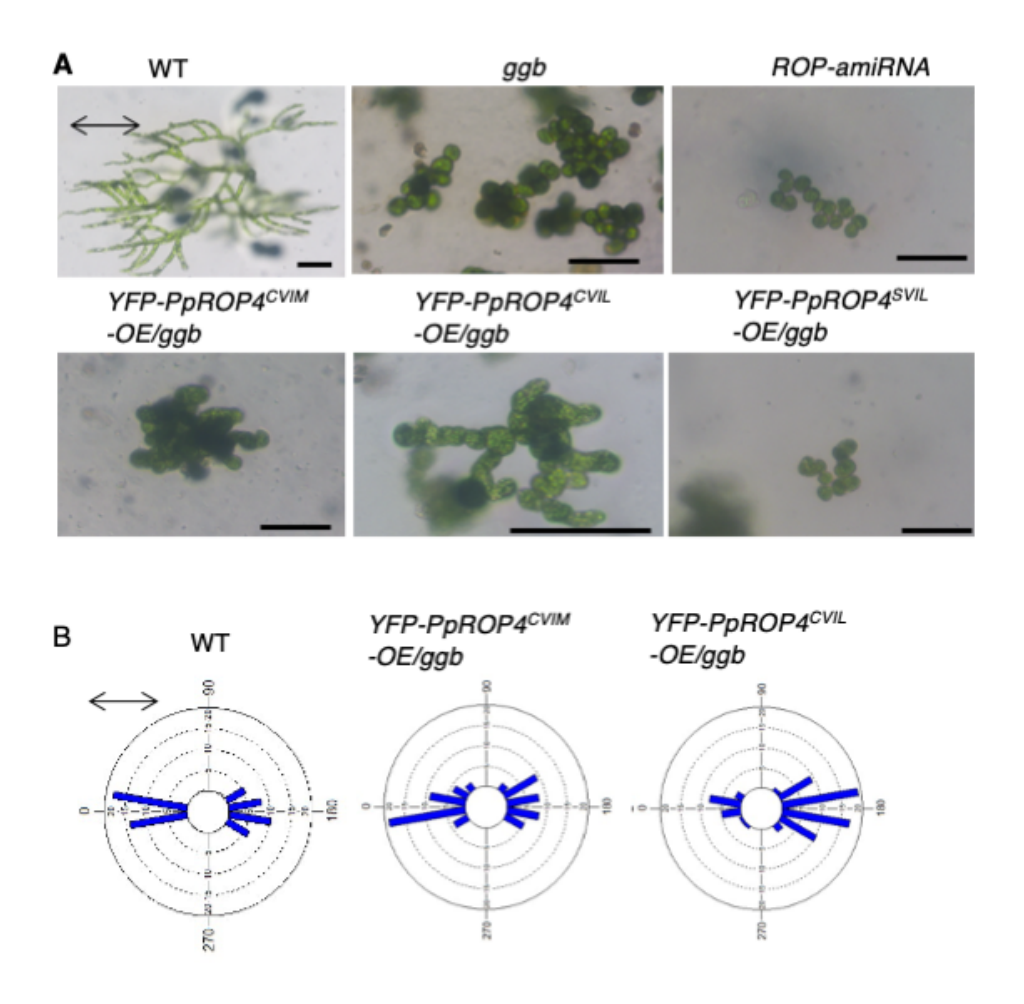


Fig. S5. Quantitative analysis of YFP-PpROP4<sup>CVIM</sup>-OE, YFP-PpROP4<sup>CVIL</sup>-OE and YFP-PpROP4<sup>SVIL</sup>-OE effect on cell expansion in WT (A) and tip growth in ggb mutants (B).

A, Measurements of cell length and cell width in apical cells. While the cell width is greater in YFP-PpROP4<sup>CVIM</sup>-OE/WT and YFP-PpROP4<sup>CVIL</sup>-OE/WT compared to YFP-PpROP4<sup>SVIL</sup>-OE/WT and WT, the cell length is smaller in YFP-PpROP4<sup>CVIM</sup>-OE/WT and YFP-PpROP4<sup>CVIII</sup>-OE/WT

compared to *YFP-PpROP4*<sup>SVIL</sup>-*OE/WT* and WT. **B**, 52 plants in each of *YFP-PpROP4*<sup>CVIM</sup>-*OE/ggb* and *YFP-PpROP4*<sup>CVIL</sup>-*OE/ggb* and *YFP-PpROP4*<sup>SVIL</sup>-*OE/ggb* were counted if they contain at least three cells that are linearly connected. Note that most plants in *YFP-PpROP4*<sup>CVIM</sup>-*OE/ggb* and YFP-*PpROP4*<sup>CVIL</sup>-*OE/ggb* formed filamentous cells, while *YFP-PpROP4*<sup>SVIL</sup>-*OE/ggb* did not. Scale bar: 200 μm (**upper**) and 50 μm (**lower**).



**Fig. S6.** Prenylation of ROP GTPase is responsible for tropic response to external light signal **A**, Shown are representative images of wild type, *ggb* mutant and transgenic plants overexpressing *ROP-amiRNA* in WT background, and overexpressing YFP-PpROP4<sup>CVIM</sup>, YFP-PpROP4<sup>CVIL</sup>, and YFP-PpROP4<sup>SVIL</sup> in *ggb* mutant background. The protoplasts regenerated under polarized white light for 27 days. Note that overexpressing PpROP4<sup>CVIM</sup> and PpROP4<sup>CVIL</sup> rescued polartropism defects of *ggb* mutant while PpROP4<sup>SVIL</sup> did not. Two-headed arrows indicate the E-vector. Scar bar:100 μm. **B**, Protonemata distributions of WT (n=61) and *YFP-PpROP4<sup>CVIM</sup>-OE/ggb* (n=70) and *YFP-PpROP4<sup>CVIL</sup>-OE/ggb* (n=75) under polarized white light.

#### Table S1. Primers

Click here to download Table S1